WELDING RESEARCH

SUPPLEMENT TO THE WELDING JOURNAL, MARCH 2001
Sponsored by the American Welding Society and the Welding Research Council

Experimental Evaluation of Fe-Al Claddings in High-Temperature Sulfidizing Environments

Assessment of Fe-Al claddings in aggressive reducing environments showed compositions with properties of weldability and high-temperature corrosion resistance

BY S. W. BANOVIC, J. N. DUPONT AND A. R. MARDER

ABSTRACT. The corrosion behavior of iron-aluminum alloys and their potential as protective corrosion claddings in sulfidizing environments were investigated. As-solidified castings of Fe-Al alloys with 0–20 wt-% Al were isothermally held at temperatures between 500 and 700°C for up to 100 h in a reducing atmosphere using thermogravimetric techniques. Specially tailored gases maintained partial pressures of oxygen and sulfur at each temperature [$p(O_2) = 10^{-25}$ atm, $p(S_2) = 10^{-4}$ atm]. Postexposure characterization of the corrosion scales consisted of surface and cross-sectional microscopy in combination with energy-dispersive spectroscopy and electron probe microanalysis. From these results, it was found the corrosion behavior was directly related to the alloys' aluminum content. For high aluminum compositions (10 wt-% Al and above), protection was afforded due to the development of a thin, continuous alumina scale that inhibited rapid attack of the alloy. Increasing the aluminum content of the alloy was found to promote the formation and maintenance of this scale, leading to excellent corrosion behavior. For low aluminum contents (<10 wt-% Al), the ability to form and/or maintain the alumina scale was not observed. Instead, thick sulfide phases developed either in the form of localized nodules (7.5 wt-% Al) or as a continuous surface scale (5 wt-% Al and below). Formation of these fast growing, nonadherent sulfide phases resulted in accelerated degradation of the alloy and unacceptable waste. With both good weldability and corrosion characteristics, alloys approaching 10 wt-% Al have excellent promise for providing protection as claddings in aggressive reducing environments.

S. W. BANOVIC, J. N. DUPONT and A. R. MARDER are with Department of Materials Science and Engineering, Lehigh University, Bethlehem, Pa.

Introduction

The choice of Fe-Al alloys in cladding applications requiring good corrosion resistance (*e.g.*, waterwall structures of coal-fired boilers with low NOx burners) is attractive due to their low cost, the lack of macro- or microsegregation upon solidification during welding (Ref. 1) and better corrosion resistance compared to conventional Ni-based and stainless steel-type compositions presently in use (Refs. 1–11). In addition, it would eliminate the brittle martensitic region that develops in the partially mixed zones of the above-mentioned austenitic alloys (Ref. 12). To date, their use is limited due to weldability issues stemming from cold cracking (Refs. 1, 13–16) and their lack of corrosion characterization in aggressive reducing environments at boiler service temperatures (typically below 700°C). In light of these facts, research was initiated to examine the sulfidation behavior of weldable Fe-Al compositions in highly aggressive reducing atmospheres. From a previous study (Ref. 1), alloys with 10 wt-% Al were identified as being readily weldable under normal field applications (Fig. 1) and had excellent corrosion behavior in moderately reducing atmospheres (Refs. 1, 13). While increasing the aluminum content has been shown to improve the corrosion resistance (Refs. 1–11), these compositions were not weldable. Some investigations (Refs. 15, 17) have cited the use of preheat and postweld heat treatments (PWHT) to relieve part of the hydrogen cracking problems, thus allowing for crack-free claddings with higher aluminum contents; however, the employment of such extensive treatments is not practical when coating large-scale structures such as utility boilers. Therefore, the objective of this work was to further characterize the corrosion behavior of weldable Fe-Al composi-

KEY WORDS

Corrosion Resistance
Cladding
Iron-Aluminum Alloys
Boilers
Sulfidizing Environment

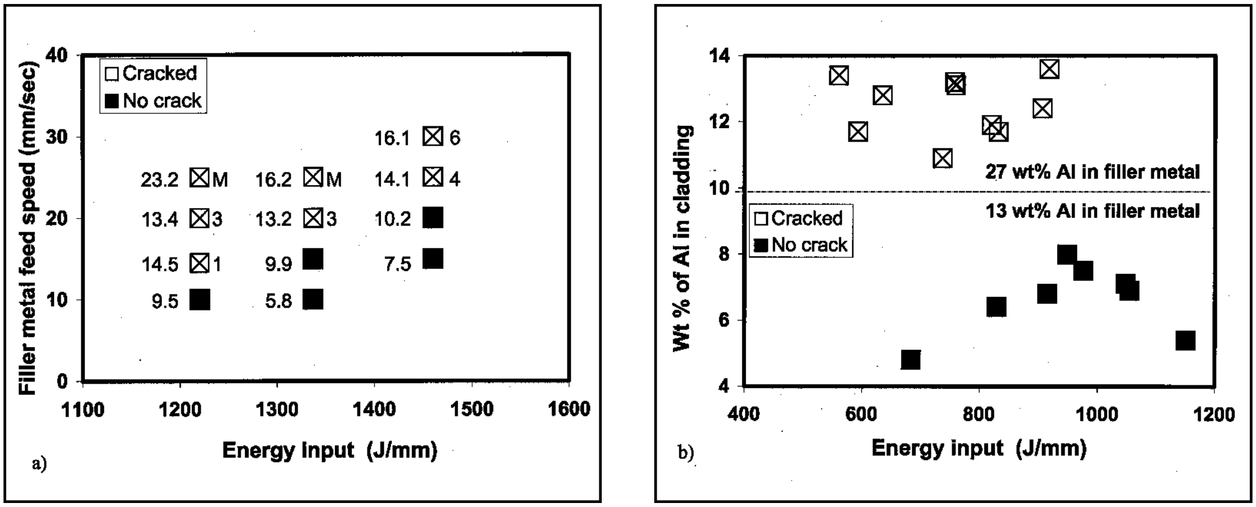

Fig. 1 — Sample matrix of multiple-pass welds. A — Gas tungsten arc welding (GTAW); B — gas metal arc welding (GMAW). Each box represents a sample deposited at that processing condition and was subsequently labeled as cracked or not cracked. For GTAW, numbers to the right of the cracked data points signify the number of cracks that occurred, with M being more than 15. The numbers to the left denote the wt-% of aluminum in the deposit (Ref. 1).

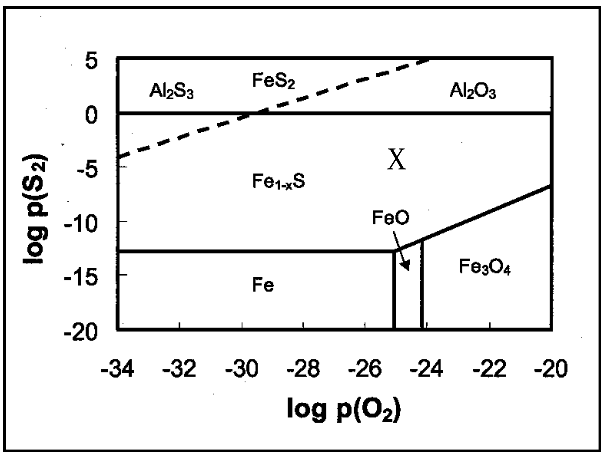

Fig. 2 — Superimposed thermostability diagrams for Fe and Al at 600°C. The solid lines represent equilibrium boundaries between the iron-based phases and the dashed line between the aluminum-based phases. The partial pressure of oxygen and sulfur place the testing environment in a region of aluminum oxide and iron sulfide ($Fe_{1-x}S$), as indicated by X. (Diagrams calculated using Ref. 21.)

tions in more aggressive reducing environments at service temperatures. The results of this work permitted these alloys to be evaluated for possible use in cladding applications that require a combination of good weldability and corrosion protection in aggressive sulfidizing atmospheres.

Experimental Procedure

The materials used in this study were a series of monolithic, iron-based alloys with varying amounts of aluminum (5, 7.5, 10, 12.5, 15 and 20 wt-% Al). These compositions were chosen based upon the previous weldability study — Fig. 1. All Fe-Al alloys were produced at Oak Ridge National Laboratory (Oak Ridge, Tenn.) by arc melting high-purity Fe (99.99%) and Al (99.99%) under argon and drop casting into a water-cooled copper mold. For comparison, a low-carbon steel alloy with 0.05 wt-% C was chosen. As-solidified castings were used to study the high-temperature sulfidation behavior instead of actual cladding material in order to eliminate the timely procedure of extracting a corrosion coupon from a deposited cladding. In addition, the aluminum-depleted region near the cladding-substrate interface, produced due to poor mixing during the welding process (Ref. 1), will be avoided. Prior research (Ref. 7) demonstrated that the corrosion products more readily formed on the specimen face located closer to the substrate due to the inhomogeneous composition (lower aluminum content) in this area. This was found to result in higher corrosion rates of the specimen. Furthermore, it was also shown the sulfidation behavior of Fe-Al claddings in reducing environments could be explained on the basis of what was known from cast alloys of equivalent compositions (Ref. 7). The reason for this stems from the fact the microstructure and distribution of alloying elements in the monolithic alloys and the claddings are essentially identical (Ref. 1) and, therefore, should have similar behavior/reactions in the corrosive atmosphere. Thus, based upon these experimental observations, the use of as-cast alloys to study the corrosion behavior of claddings of identical compositions is clearly justified.

For the corrosion testing, substrates with dimensions of 1 cm x 1 cm x 2 mm were sectioned from the bulk using a high-speed diamond saw. Subsequent grinding of the surface to 600 grit was also conducted. Specimens were prepared immediately before insertion into the balance with prior steps of ultrasonic cleaning in soapy water and methanol. A Netzsch STA 409 high-temperature thermogravimetric balance was used to measure weight gain as a function of time, with the gas compositions and temperatures chosen so as to produce a highly reducing environment indicative of low NOx gas conditions (Refs. 18–20). Samples were heated at a rate of 50°C/min and isothermally held at temperatures of 500, 600 and 700°C for various times (1, 5, 15, 25, 50 and/or 100 h). Mixtures of H_2-H_2S-O_2-Ar gases were determined so as to maintain equivalent partial pressures for oxygen, $p(O_2)$, and sulfur, $p(S_2)$, at different temperatures. Table 1 shows the gas compositions, as reported by Scott Specialty Gases, and the corresponding $p(O_2)$ and $p(S_2)$ values for each temperature. The $p(O_2)$ was determined using a solid-state oxygen detector and the $p(S_2)$ was calculated using the SolGasMix program (Ref. 21). According to superimposed thermostability diagrams for iron and aluminum at test temperatures, the location of the testing environment was found to lie in a region of aluminum oxide and iron sulfide ($Fe_{1-x}S$). These stability diagrams will indicate which phases (*e.g.*, Fe, Al, alumina, iron sulfide) are thermodynamically stable on all of the alloy's surface for the given testing parameters; they do not indicate which scales will actually be observed to form. An example of one developed at 600°C is shown in Fig. 2, with the location of the testing parameters denoted by X. The present gas mixtures chosen were more aggressive than those used during the early study (Ref. 1) in which only moderately reducing atmospheres were investigated. For comparison, the composition, $p(O_2)$, and $p(S_2)$ of this previously used gas is also shown in Table 1.

Postexposure characterization of the corroded surfaces was conducted using a JEOL 6300F scanning electron microscope with an Oxford (Link) energy-dispersive spectroscopy (EDS) system capable of detecting light elements. Polished cross-sections were obtained by mounting in cold setting epoxy with subsequent grinding procedures to 1200 grit with silicon-carbide papers. A final polishing step was conducted using 1-µm diamond paste on a low-nap cloth. Further polishing with any type of colloidal alumina or silica was avoided to minimize the possibility of contamination or pull-out of the scale. Cross-sectional scale thicknesses were measured on electron micrographs using a digitizing pad interfaced with a Nikon Optiphot microscope. A minimum of 20 lengths were taken per layer per sample on various planes. Quantitative chemical information was obtained on polished cross-sections using a JEOL 733 electron probe microanalyzer (EPMA) equipped with wavelength-dispersive spectrometers (WDS). The accelerating voltage and probe current were 20 kV and 50 nA, respectively. K_α X-ray lines were analyzed and counts converted to wt-% using a $\phi(\rho z)$ correction scheme (Ref. 22).

A fracturing technique using liquid nitrogen was also employed to view the scales in cross-section. By notching the back side (approximately ⅘ of the thickness of the substrate) with a low-speed diamond saw and submersing the specimen for a minimum of 3 min in liquid nitrogen, the samples easily broke. Cross-sectional micrographs of these samples were also taken using the JEOL 6300F.

Results

Corrosion Kinetics

Figure 3 displays the kinetic results obtained at each temperature for the longest exposure time for each alloy. In all cases, shorter time exposures (1, 5, 15 and 25 h) followed their respective weight gain data curves for the longer times with good reproducibility. From this data, a general trend was observed that an increase in aluminum content produced a decrease in the weight gain, and once above 7.5 wt-% Al, the increase was relatively small. It was also noted that an increase in temperature from 500 to 600°C led to a decrease in weight gain for alloys with less than 10 wt-% Al, while the increase from 600 to 700°C produced a significant increase in the weight gain.

Corrosion Morphologies

As a general trend, increasing the aluminum content led to decreased amounts of corrosion product on the surface. For the low-carbon steel sample, a thick, bilayered scale was found — Fig. 4. The outer scale appeared to be dense and columnar with the inner scale being fine-grained and porous. EPMA data (Table 2) indicated both layers were iron sulfide ($Fe_{1-x}S$), with separation between these two morphologies. This separation indicated poor adhesion between these two morphologies and, on occasion, resulted in scale spallation prior to mounting. The 5 wt-% Al alloy also grew a continuous surface scale

Table 1 — Corrosion Gas Compositions and Corresponding Partial Pressures of Oxygen (Measured) and Sulfur (Calculated) at Temperature

Gas Composition (by volume)	Temp (°C)	$p(O_2)$ (atm)	$p(S_2)$ (atm)
$1.1\%H_2S$-$0.0\%H_2$-$98.9\%Ar$ (500 ppm O_2)	500	9.2×10^{-26}	7.5×10^{-4}
$0.9\%H_2S$-$0.0\%H_2$-$99.1\%Ar$ (50 ppm O_2)	600	7.4×10^{-25}	4.0×10^{-4}
$1.0\%H_2S$-$0.1\%H_2$-$98.9\%Ar$ (5 ppm O_2)	700	3.4×10^{-25}	5.4×10^{-4}
$0.1\%H_2S$-$3.0\%H_2$-$96.9\%Ar$ (5 ppm O_2) (previous study)(a)	600	4.5×10^{-28}	3.8×10^{-9}

(a) From Ref. 1.

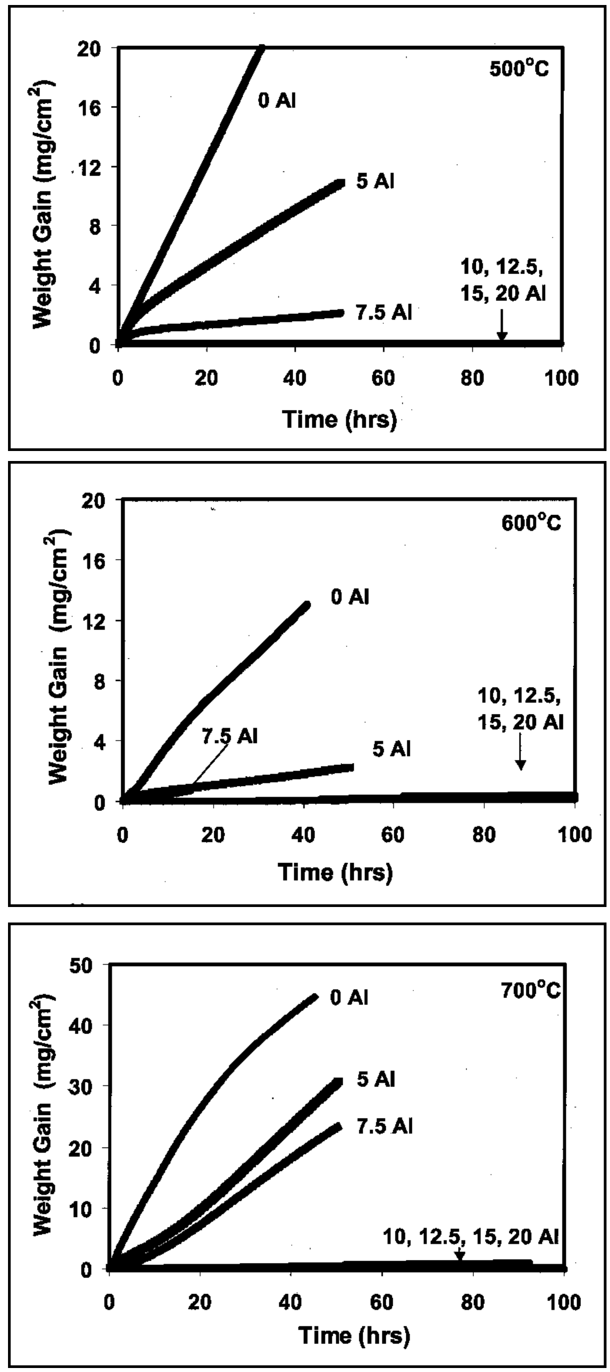

Fig. 3 — Weight gain vs. time for various exposure temperatures at $p(O_2) = 10^{-25}$ atm and $p(S_2) = 10^{-4}$ atm. A — 500°C; B — 600°C; C — 700°C.

Table 2 — Representative EPMA Data, Reported in Weight Percentages, for Thick Sulfide Phases Taken from the Low-Carbon Steel and Fe-5 wt-% Al Alloy

Sample	Scale Feature	Fe	Al	S	Phase(s)
Low-carbon steel	Outer scale	61.7 ± 0.5	0.0	37.7 ± 0.3	$Fe_{1-x}S$
Low-carbon steel	Outer scale	61.7 ± 0.8	0.0	37.5 ± 0.5	$Fe_{1-x}S$
Fe-5 wt-% Al	Outer scale	61.7 ± 0.5	0.9 ± 0.2	37.6 ± 0.4	$Fe_{1-x}S$
Fe-5 wt-% Al	Scan of inner layer	45.1± 0.3	8.3 ± 0.5	43.3 ± 0.7	$\tau + Fe_{1-x}S$
Fe-5 wt-% Al	Dark, inner layer plate	24.0 ± 0.8	20.7 ± 0.3	52.8 ± 1.0	τ
Fe-5 wt-% Al	Substrate near scale	95.4 ± 0.3	4.9 ± 0.1	0.0	α-(Fe)
Fe-5 wt-% Al	Alloy at far distances	95.7 ± 0.3	4.9 ± 0.5	0.0	α-(Fe)

that was bilayered — Fig. 5. Quantitative chemical analysis (Table 2) showed the outer scale consisted of irregularly shaped iron sulfide ($Fe_{1-x}S$) plates, and the inner scale was found to be a two-phase mixture of τ-phase platelets ($FeAl_2S_4$), a spinel-type compound (dark in Fig. 5B) and $Fe_{1-x}S$ particles (light particles in Fig. 5B). Sampling of the inner layer as a whole was obtained by scanning areas of approximately 25 µm^2. The results placed it in the two-phase region of τ and $Fe_{1-x}S$ on the ternary phase diagram — Fig. 6. Porosity in the inner scale was also found (black in Fig. 5B). In the alloy located next to the inner scale, depletion of either metallic element (Fe, Al) or the ingress of sulfur into the alloy was not observed, within the detection limits of the electron microprobe equipment (~1 µm). In addition, it was observed that the sulfide scales of the above-mentioned samples exhibited poor adherence to the alloy and easily flaked off during handling.

With compositions of 10 wt-% Al and above, the samples did not develop the thick, surface corrosion products that were found on the previous specimens. Instead, electron micrographs of the surfaces revealed continuous coverage by a granular scale (Fig. 7A) that had the appearance of either a tan, blue or purple color to the naked eye. Qualitative analysis by EDS indicated high counts of Al and O with minor amounts of Fe and S — Fig. 7B. Fractured cross-sectional micrographs in these areas were also obtained (Fig. 7C) with arrows denoting the scale. It appeared to be uniform across the sample with the cross-sectional thickness having a relationship with both time and temperature — Fig. 8. However, changes in aluminum content for a given testing condition did not lead to significant differences in scale morphology or thickness.

Samples with 7.5 wt-% Al were found to develop localized sulfide growths that were randomly dispersed across the surfaces — Fig. 9. These nodules had a similar appearance regardless of the exposure time and temperature. Exposures above 15 h led to the coalescence of some of the nodules, and, as they were well dispersed across the sample face, it did not appear that the substrate grain boundaries played a major role in their location. A granular surface scale, similar to the one found on the higher aluminum alloys, was present in the nodule-free areas — Fig. 9C. Cross-sectional analysis (Fig. 9D) showed the nodules consisted of similar phases as seen in the thick scale growths. The overall appearance had a lenticular shape with further analysis revealing an outer scale of thick $Fe_{1-x}S$ plates with various growth directions. The inner scale was also composed of τ-phase platelets and $Fe_{1-x}S$ particles that developed normal to the surface. In the substrate directly below the nodules, EPMA analysis did not indicate the presence of sulfur or the depletion of either metallic element. The same can be said for the alloy located below the thin granular scale.

Discussion

The corrosion behavior of weldable Fe-Al alloys, for use as protective corrosion claddings in oxidizing-sulfidizing environments, was studied through thermogravimetric methods with the resulting corrosion scales characterized by microscopy techniques and chemical analysis. The alloy compositions were chosen based on previous weldability studies (Ref. 1) that indicated Fe-Al alloys with 10 wt-% Al or less were readily weldable under typical field applications — Fig. 1. Therefore, compositions on both sides of this weldability limit were evaluated with respect to their corrosion characteristics. From these experiments, it was found the corrosion behavior of these alloys was directly related to the aluminum content of the sample. This variable dictated the type (oxide/sulfide), morphology and amount of corrosion product that formed during high-temper-

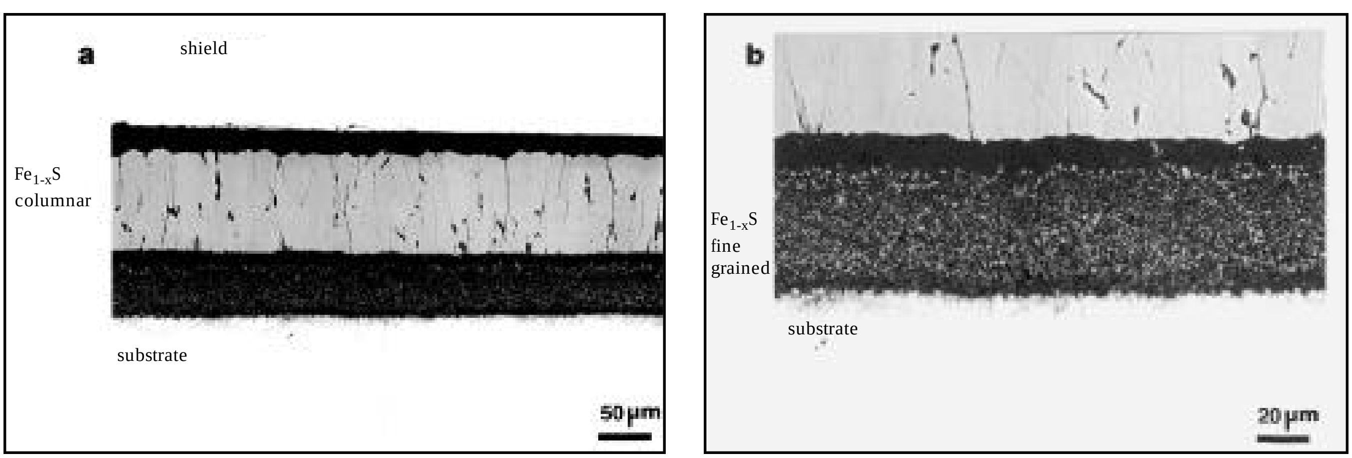

Fig. 4 — Light optical micrograph of a polished cross-section showing the scale that developed on the low-carbon steel sample after 50 h at 600°C. A — Full scale; B — higher magnification of the inner scale with separation between the two morphologies.

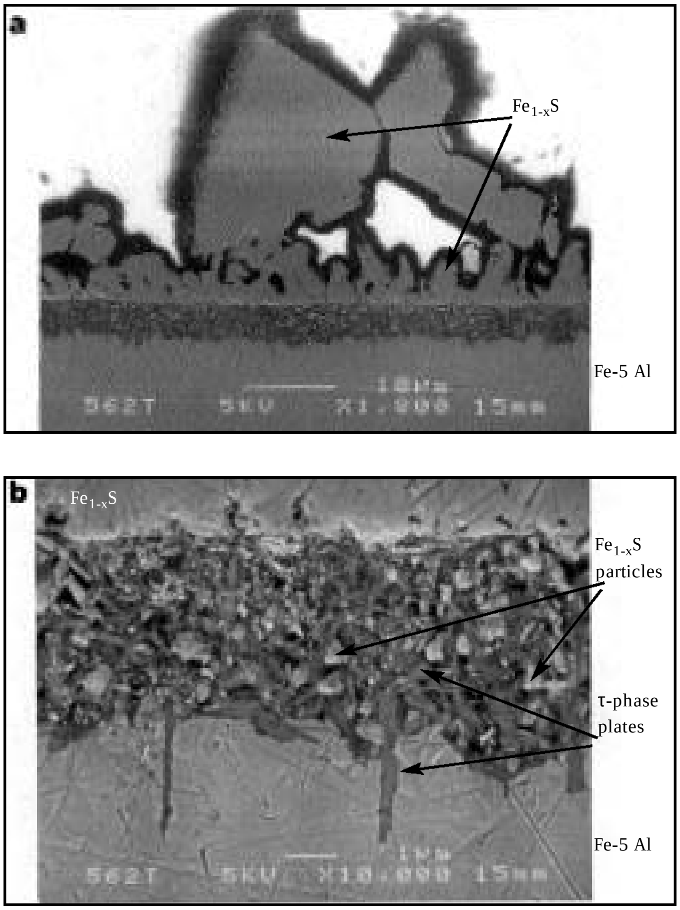

Fig. 5 — Secondary electron image of a polished cross-section showing the bilayered scale that formed on the 5 wt-% Al sample after 50 h at 600°C. A — Full scale; B — higher magnification of the inner scale showing τ-phase platelets and $Fe_{1-x}S$ particles.

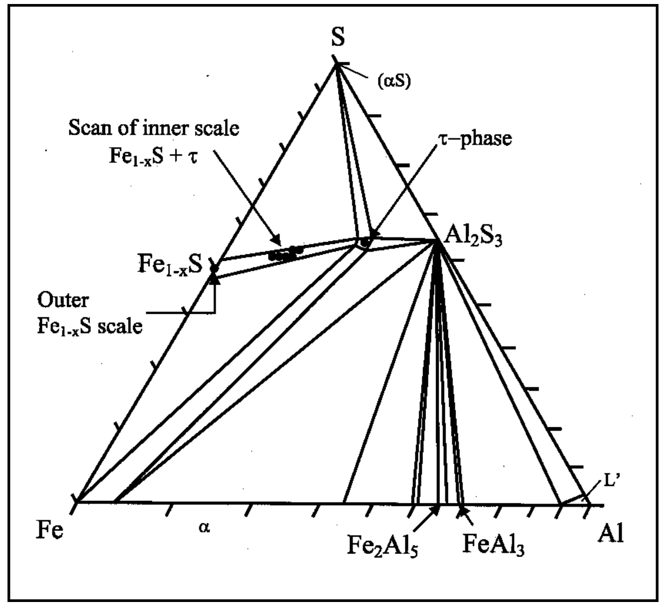

Fig. 6 — Fe-Al-S ternary phase diagram at 900°C with overlaid EPMA data for the corrosion products and underlying substrate (Ref. 36). Axes are in weight percentages.

ature exposure in the reducing atmosphere. These growths were typically in the form of a surface scale or scales that developed with time. As a general trend, increasing the amount of aluminum in the alloy led to decreased corrosion rates and the amount of corrosion product. These results are discussed below as they relate to the prospect of using Fe-Al compositions as corrosion protective claddings.

Additions of aluminum at 10 wt-% and above were found to decrease the corrosion rates by promoting the formation of a slow-growing surface scale on the alloy during exposure. The low weight gain data obtained during corrosion testing was indicative of this fact — Fig. 3. The surface scales were composed of tightly packed, equiaxed grains of an aluminum- and oxygen-rich scale — Fig. 7. While definitive identification of the scale could not be made, enough evidence suggests it is an aluminum oxide, probably γ-alumina, in terms of the EDS analysis, color (Ref. 23) and temperature regime in which it has formed (Ref. 24), and its protective nature (low weight gain and thickness). In addition, numerous researchers working on similar alloys have also found protection due to γ-alumina scales in these types of mixed oxidizing-sulfidizing environments (Refs. 3–5). Other surface characterization techniques, such as grazing incidence X-ray diffraction (GIXRD) and backscatter electron kikuchi patterns (BEKP), were used in an attempt to identify the scales. Unfortunately, results from these analyses could not confirm the crystal structure. In any event, this scale formed due to preferential oxidation of the aluminum on the alloy surface, and the results indicated that formation of this scale was promoted through increasing the aluminum content of the alloy.

When the aluminum content was decreased to 7.5 wt-% or lower, thick sulfide phases were found to develop either in the form of nodules or a continuous surface scale due to the lack of aluminum at the surface. The growth of these corrosion products was found to be diffusion controlled, predominantly through the outward movement of Fe cations, to form an external layer of iron sulfide ($Fe_{1-x}S$), and the inward diffusion of sulfur, as indicated by the inner scale development of τ-phase platelets and $Fe_{1-x}S$ particles. For the 7.5 wt-% Al sample, initial formation of the alumina scale was observed, as indicated by the granular scale in the nodule-free areas — Fig. 9C. At extended times, mechanical failure of this scale, and the inability to heal itself due to the low Al content of the alloy, led to the short-circuit diffusion of sulfur through the passive layer (Ref. 25). This resulted in the subsequent growth of the sulfide phase at the alumina scale/alloy interface. The higher nominal aluminum compositions did not experience this failure as sufficient amounts of aluminum were located at the surface to repair the breakdown in the scale. As the nominal aluminum content of the alloy was further decreased to 5 wt-% and lower, the formation of a protective alumina scale was not observed. Instead, thick scale growths accompanied by relatively high weight gains were found from the onset of exposure, which led to excessive degradation of the alloy. This type of scale formation would lead to rapid deterioration of the cladding as the morphologies were porous and observed to readily spall. Eventually, this would result in the corrosive gas having direct access to the underlying tube material after the cladding material was completely consumed by the corrosion process.

From these results, it appears the Fe-Al compositions that perform well in the reducing environments are alloys that formed the surface scale of alumina. The protectiveness of this thermally grown oxide manifested itself in two ways: 1)

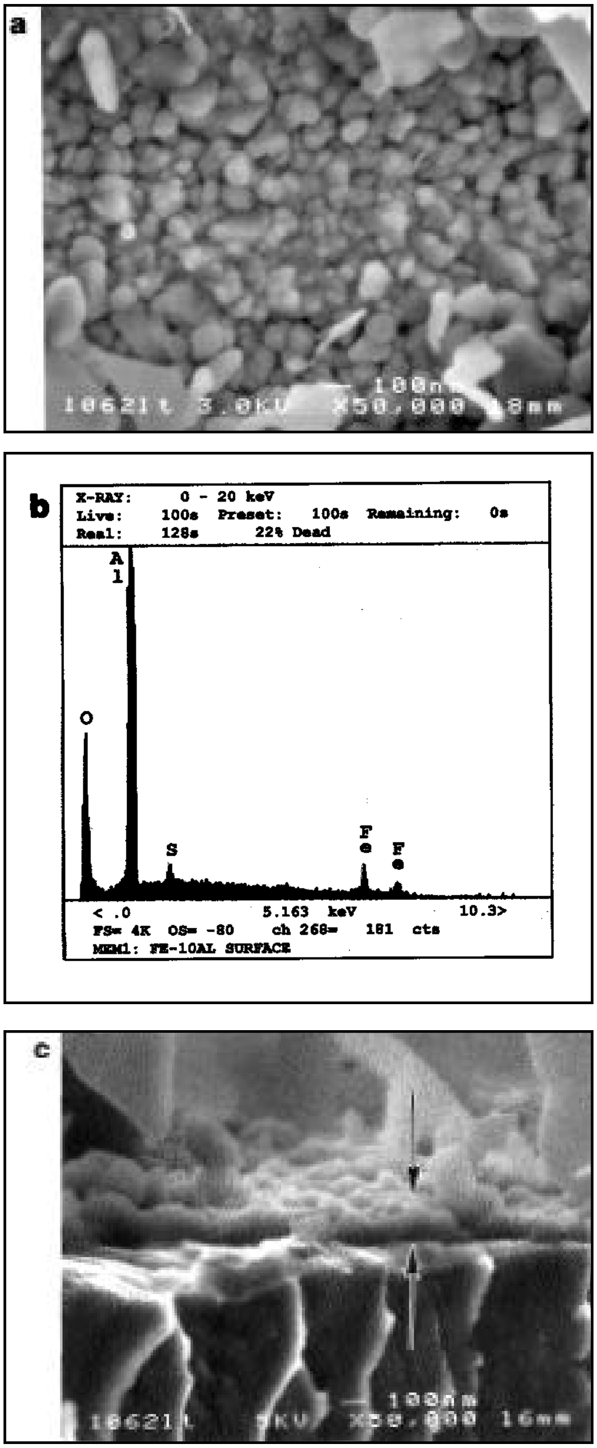

Fig. 7— Characteristic secondary electron image of the granular surface scale formed on alloys of 10 wt-% Al or higher after 100 h at 600°C. A — Surface morphology; B — the associated EDS spectrum; C — fractured cross-section with arrows indicating thickness of alumina scale. Sample shown is Fe-10 wt-% Al.

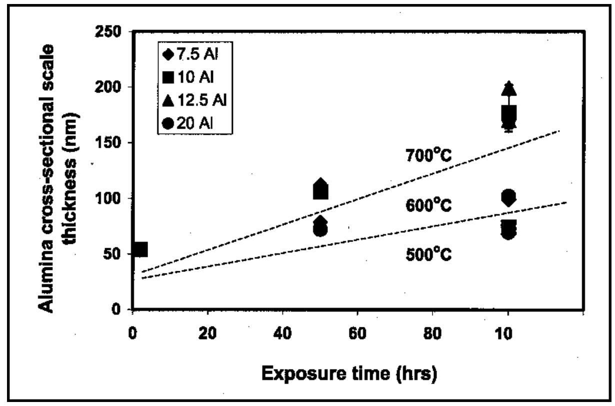

Fig. 8 — Cross-sectional alumina scale thickness as a function of time and temperature (ranges indicated by dashed lines) for various aluminum contents.

low weight gains and corresponding thinness of scale and 2) lack of sulfur ingress into the alloy. While it is intuitive that formation of a protective scale will result in lower weight gains from reduced attack of the alloy, it is also important to note the thickness of the scale providing protection at temperature. The alumina scales observed to grow on the weldable compositions (10 wt-% Al) barely attained 100 nm of growth at 600°C over the 100-h exposure period, yet were able to maintain less than 0.5 mg/cm^2 in weight gain. Other alumina scales, with different crystal structures, also provide protection at higher temperatures, but have a tendency to become much thicker over time even though their weight gains are also relatively low. As an example, another phase of alumina, α, provides protection for iron aluminide compositions above 1000°C. At exposure temperature, these scales can grow to a thickness of 8 µm within 100 h (Ref. 26). Preferential aluminum removal through thick scale growth depletes the alloy of this element at a relatively fast rate, and, after long times, the nominal aluminum composition of the alloy can drop to significantly low levels.

Rapid consumption of aluminum due to alumina scale growth is critical when considering the Fe-Al alloys for use as protective claddings, as the weldable compositions considered here have relatively low aluminum reserves to begin with. In terms of the corrosion resistance, the effectiveness of a cladding can be defined by the oxidation lifetime, or the amount of time over which a surface scale (such as alumina) will be maintained to provide protection for the underlying material. This concept was studied and modeled by Quadakkers, *et al.* (Refs. 27, 28), and recently reviewed by Tortorelli and Natesan (Ref. 29). The time frame for protection has been found to be a function of the total amount of aluminum available for reaction (at the surface and in reserve within the bulk) and the rate at which it is consumed. The effective lifetime of a cladding ends when the aluminum content falls below a composition such that continuous formation of the alumina scale is not possible and the development of less protective products, such as sulfide phases, can occur, leading to high wastage rates.

Through the use of Fe-Al alloys as protective claddings, the reservoir of aluminum in the deposit will automatically be limited due to the thickness of the deposited cladding, typically 1–2 mm. Therefore, it is natural to conclude that increasing the nominal aluminum content of the deposit will further increase the potential effective lifetime of the protective coating. However, it has been shown a limit (approximately 10 wt-% Al) is imposed on the system in order to produce sound claddings deposited under conditions typically utilized in practice — Fig. 1. Aluminum contents above this value have been found to be susceptible to cold cracking subsequent to welding (Refs. 1, 13–16), with the severity of the problem increasing with aluminum content (Refs. 1, 30–32). Cracking of the cladding would enable the corroding specie to have direct access to the less corrosion-resistant substrate, typically a low-alloy steel, allowing for high corrosion rates. Consequently, without the option of in-

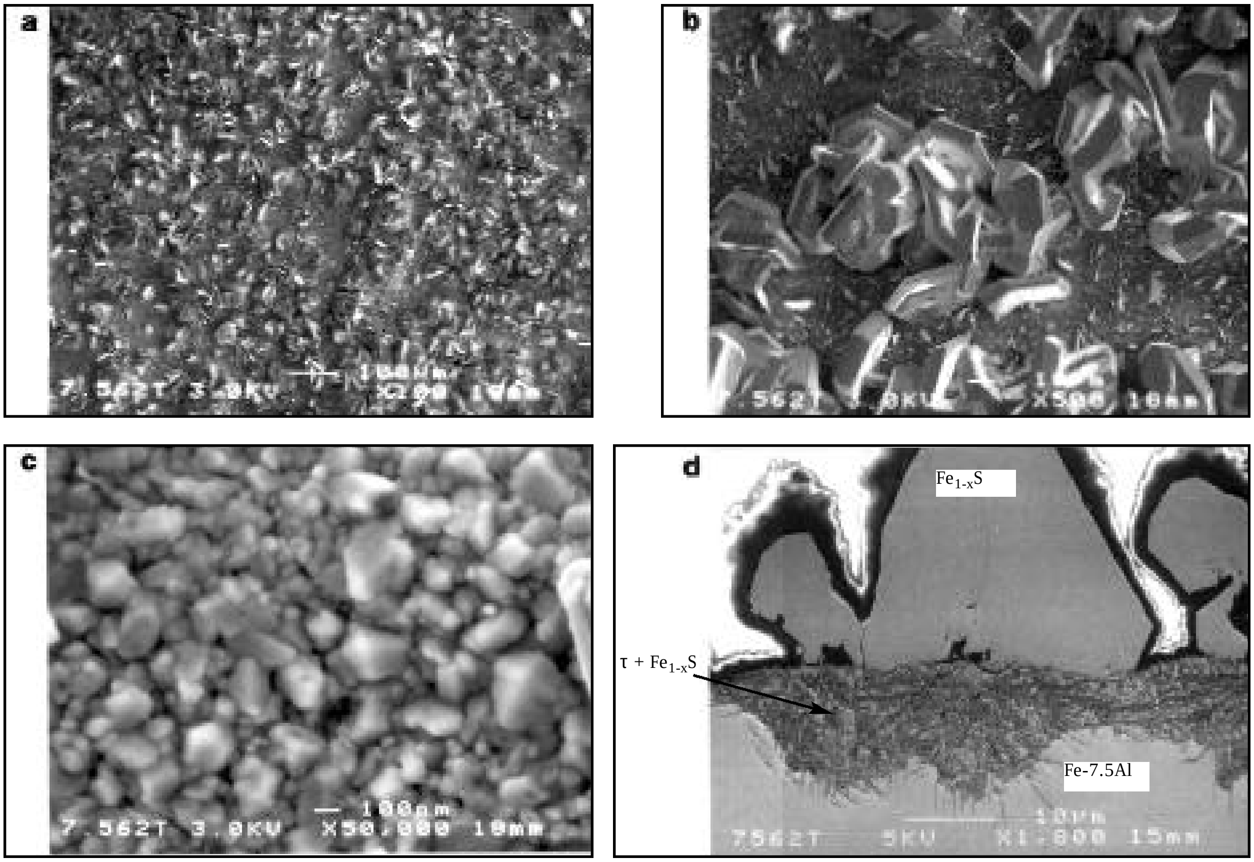

Fig. 9 — Secondary electron images of the surface scale developed on alloys with 7.5 wt-% Al after 50 h of exposure at 600°C. A and B — Nodule sulfide phases on the surface; C — granular scale in the nodule-free region; D — polished cross section of the nodules.

creasing the nominal aluminum content of the deposit, the other alternative to increasing the effective lifetime of weldable compositions is by reducing the rate at which aluminum is consumed. In this study, it was shown through the thickness (thinness) of the scale that the rate of aluminum consumption at these test temperatures was very low — Fig. 8. In addition, this thinness may be beneficial in that large growth stresses, which could enhance spallation of the scale during thermal cycling, may not have developed. This spallation is detrimental in that it would lead to faster consumption rates of aluminum as the scale must now reform. While thermal cycling of the specimens was not conducted nor stress measurements of the scale made during this phase of the work, at no time was the alumina scale ever observed to crack, spall or flake off, even after fracturing in liquid nitrogen (for samples with 10 wt-% Al or higher). This suggests an adherent scale. Therefore, the thinness of the scale over extended periods of time, combined with the lack of spallation, results in a very low rate of aluminum consumption and suggests these alloys will provide protection for extended periods of time at application temperatures (around 500°C).

While the alumina scale was able to maintain low weight gains for long times, it was also protective in the fact that internal sulfidation of the alloy did not occur. Microprobe traces near the alloy-scale interface did not detect an increase in sulfur when compared to far distances into the substrate, which suggests the scale was somewhat dense and impervious to inward diffusion of the anion. This may be related to the fact that γ–alumina primarily grows via an outward cation diffusion mechanism (Refs. 24, 33) and not an inward anion diffusion as predominately found for α-alumina scale formation (Ref. 34). Sulfur penetration can be disastrous to the protective scale due to the formation of sulfide phases beneath its surface, which can lead to mechanical degradation of the passive layer, as found for the 7.5 wt-% Al alloy. However, the corrosion behavior observed here suggests this should not be a problem for these higher-aluminum-content alloys.

As a final note, it was observed that increasing the exposure temperature did not produce a trend in the weight gain data. Whereas corrosion rates were accelerated by increasing the temperature from 600 to 700°C, exposures at 500°C produced higher weight gains than at 600°C. This was unexpected as diffusional processes are thermally activated, and thus, should decrease in magnitude as the temperature is decreased (Ref. 35). Therefore, another mechanism may be controlling the growth of these sulfide scales in this temperature regime (500°C) and work is currently under way to investigate this apparent anomaly.

Summary

The objective of the present study was to investigate the corrosion behavior of weldable compositions of iron-aluminum alloys in sulfidizing environments indicative of low NOx gas compositions. From this work, it was observed the corrosion behavior was directly related to the aluminum content of the alloy. For high aluminum compositions (10 wt-% Al and above), protection was afforded due to the development of a thin, continuous alumina scale that inhibited rapid degradation of the alloy. Increasing the aluminum content facilitated the formation and maintenance of this scale. Alloy contents at or below 7.5 wt-% Al led to high waste rates due to the formation of thick sulfide phases that were friable. With these results, weldable compositions of Fe-Al alloys show the potential promise for applications requiring a combination of weldability and corrosion resistance in aggressive sulfidizing conditions. Therefore, these alloys are viable candidates for further evaluation for use as corrosion-resistant coatings.

Acknowledgments

This research was sponsored by the Fossil Energy Advanced Research and Technology Development (AR&TD) Materials Program, U.S. Department of Energy, under contract DE-AC05-96OR22464 with Lockheed Martin Energy Research Corp. The authors wish to thank V. K. Sikka and P. F. Tortorelli from ORNL for the cast-Fe-Al alloys used in corrosion testing and technical discussions, respectively.

References

1. Banovic, S. W., DuPont, J. N., P. F. Tortorelli, and Marder, A. R. 1999. The role of aluminum on the weldability and sulfidation behavior f iron-aluminum cladding. *Welding Journal* 78(1): 23-s to 30-s.

2. McKamey, C. G., DeVan, J. H., Tortorelli, P. F., and Sikka, V. K. 1991. *J. Mater. Res*. 6 (8): 779–805.

3. DeVan, J. H., and Tortorelli, P. F. 1993. *Mater. High Temp*. 11(1–4): 30–35.

4. Tortorelli, P. F. and DeVan, J. H. 1992. *Mater. Sci. and Eng.*, A135 (1–2): 573–577.

5. DeVan, J. H. 1988. *Oxidation of High Temperature Materials*, eds. T. Grobstein and J. Doyhak. TMS, Cleveland, Ohio, pp. 107–115.

6. Natesan, K. 1997. *Proceedings of the Eleventh Annual Conference on Fossil Energy Materials*, pp. 289–299. Oak Ridge National Laboratory, Oak Ridge, Tenn.

7. Tortorelli, P. F., Goodwin, G. M., Howell, M., and DeVan, J. H. 1995. *Heat-Resistant Materials II*, pp. 585–590. ASM International, Materials Park, Ohio.

8. Tortorelli, P. F., DeVan, J. H., Goodwin, G. M., and Howell, M. 1994. *Elevated Temperature Coatings: Science and Technology I*, pp. 203–212. TMS, Warrendale, Pa.

9. DeVan, J. H., and Tortorelli, P. F., 1992. High temp. corr. of iron aluminides. *Corrosion 92*, Paper 127.

10. Kai, W., and Huang, R. T. 1997. *Oxid. Met.*, 48(1/2): 59–86.

11. Kai, W., Chu, J. P., Huang, R. T., and Lee, P. Y. 1997. *Mater. Sci. Engr.* A239–240, pp. 859–870.

12. Gittos, M. F., and Gooch, T. G. 1992. The interface below stainless steel and nickel-alloy claddings. *Welding Journal* 71(12): 461-s to 472-s.

13. Banovic, S. W., DuPont, J. N., and Marder, A. R. 1998. *Scripta Metall* 38(12): 1763–1767.

14. David, S. A., Horton, J. A., McKamey, C. G., Zacharia, T., and Reed, R. W. 1989. Welding of iron aluminides. *Welding Journal* 68(9): 372-s to 381-s.

15. Maziasz, P. J., Goodwin, G. M., Liu, C. T., and David, S. A. 1992. *Scripta Metall.* 27(12): 1835–1840.

16. Fasching, A. A., Ash, D. I., Edwards, G. R., and David, S. A. *Scripta Metall.* 32(3): 389–394.

17. David, S. A., and Zacharia, T. 1991. Heat-resistant materials. *Proceedings of the 1st International Conference*, pp. 169–173, Fontana, Wis.

18. Chou, S. F., Daniel, P. L., Blazewicz, A. J., and Dudek, R. F. 1984. Hydrogen sulfide corrosion in low NOx combustion systems. Babcock & Wilcox report No. RDTPA 84-1, Metallurgical Society of AIME. Detroit, Mich.

19. Urich, J. A., and Kramer, E. 1996. *International Joint Power Generation Conference*, Vol. 1, pp. 25–29. ASME, EC-Vol. 4/FACT-Vol. 21.

20. Gabrielson, J. E., and Kramer, E. D. 1996. *International Joint Power Generation Conference,* Vol. 1, pp.19–23. ASME, EC-Vol. 4/FACT-Vol. 21.

21. HSC Chemistry for Windows, Version 3.0. 1997. Outokumpu Research Oy, Finland, *www.outokumpu.fi/hsc*.

22. Goldstein, J. I., *et al.* 1992. *Scanning Electron Microscopy and X-ray Microanalysis*, 2nd edition. Plenum Press, New York, N.Y.

23. Hagel, W. C. 1965. *Corros., 21*, pp. 316–326.

24. Prescott, R., and Graham, M. J., *Oxid. Met.* 38(3-4): 233–254.

25. Banovic, S. W., DuPont, J. N., and Marder, A. R. 1999. submitted to *Oxid. Met.*

26. Pint, B. A. 1997. *Mater. Sci. Forum*, pp. 251–254, 397–404.

27. Quaddakers, W. J., and Bongartz, K. 1994. *Werjst. Korros.*, 45, pp. 232–238.

28. Quaddakers, W. J., and Bennett, M. J. 1994. *Mater. Sci. Technol.*, 10: 126–131.

29. Tortorelli, P. F., and Natesan, K. 1998. *Mater. Sci. Engr.*, A285, pp. 115–125.

30. Woodyard, J. R., and Sikka, V. K. 1993. *Scripta Metall.*, 29, pp. 1489–1493 .

31. Sikka, V. K., Viswanathan, S., and Vyas, S. 1993. High temperature ordered intermetallic alloys V. *Materials Research Society Symposium Proceedings*, Vol. 28, pp. 971–976, eds. I. Baker, R. Darolia, J. D. Whittenberger, and M. H. Yoo. Materials Research Society, Pittsburgh, Pa.

32. Vyas, S., Viswanathan, S., and Sikka, V. K. 1992. *Scripta Metall.*, 27, p. 185.

33. Prescott, R., and Graham, M. J., *Oxid. Met.* 38(1–2): 73–87.

34. Pint, B. A. 1997. *Fundamental Aspects of High Temperature Corrosion*, eds. D. A. Shores, R. A. Rapp, and P. Y. Hou, pp. 74–85. Electrochemical Society, Pennington, N.J.

35. Kofstad, P. 1992. *High Temperature Corrosion*. Elsevier Applied Science, New York, N. Y.

36. Raghavan, V. 1988. *Phase Diagrams of Ternary Alloys*, Pt 2, pp. 5–9. The Indian Institute of Metals, Calcutta, India.